Fault Tolerant 7-phase Hybrid Excitation Permanent Magnet Machine

Benteng Zhao, Jinlin Gong, Duc Tan Vu, Ngac Ky Nguyen, Eric Semail

▶ **To cite this version:**

Benteng Zhao, Jinlin Gong, Duc Tan Vu, Ngac Ky Nguyen, Eric Semail. Fault Tolerant 7-phase Hybrid Excitation Permanent Magnet Machine. The Eighteenth Biennial IEEE Conference on Electromagnetic Field Computation CEFC 2018, Oct 2018, Hangzhou, China. pp.5. hal-02167379

HAL Id: hal-02167379
https://hal.science/hal-02167379v1

Submitted on 27 Jun 2019

HAL is a multi-disciplinary open access archive for the deposit and dissemination of scientific research documents, whether they are published or not. The documents may come from teaching and research institutions in France or abroad, or from public or private research centers.

L'archive ouverte pluridisciplinaire **HAL**, est destinée au dépôt et à la diffusion de documents scientifiques de niveau recherche, publiés ou non, émanant des établissements d'enseignement et de recherche français ou étrangers, des laboratoires publics ou privés.

Fault Tolerant 7-phase Hybrid Excitation Permanent Magnet Machine

B. Zhao[1], J. Gong[1], D. T. Vu[2], N. Nguyen[2], and E. Semail[2]

[1]Shandong University, School of Electrical Engineering, Jinan 250061, Shandong, China
[2] Univ. Lille, Arts et Metiers ParisTech, Centrale Lille, HEI, EA 2697 - L2EP -Laboratoire d'Electrotechnique et d'Electronique de Puissance, F-59000 Lille, France

This paper presents a novel 7-phase hybrid excitation permanent magnet (HEPM) machine with three rotors around one stator. Two rotors with PMs axially magnetized and the third rotor with PMs radially magnetized. Thanks to the addition of the third rotor, the inactive end-windings in the configuration with two rotors are then becoming active with a contribution to the torque with an increase of 30%. The impact of the third rotor on the torque density and on the pulsating torques is presented. The fault-tolerant characteristics of the proposed machine are also presented, which proves the interests of this machine for low speed applications.

***Index Terms*—fault tolerant, high torque density, hybrid excitation, 7-phase PM machine.**

I. Introduction

Multiphase machines have been gained increasing focus in critical applications, such as submarine electric propulsion, aerospace and automation traction etc., due to the fault tolerant capability, potential high torque and power density with high quality of torque [1].

The torque density of the multi-phase machine can be increased by injection of higher order of harmonics of currents. The machine in [2] can obtain 30% more of torque by designing both the shape of PM and the injection of 3rd harmonic of current. With eleven-phase induction machines, [3] obtains a 14% improvement of torque with a third harmonic injection and up to 27% with an injection of harmonics up to the 9th harmonic.

Compared to traditional machines, axial flux PM machines (AFPM) have favorable characteristics concerning high torque density for low-speed operation especially suitable for direct-drive applications, such as wheel direct-drive application [4-6]. A 7-phase AFPM was designed in [7], which proved the effectiveness of both fault-tolerant capability by controlling the harmonics of current and electromagnetic force (EMF). Based on which, a novel 7-phase machine with hybrid excitation of PMs is proposed in this paper in order to increase furtherly the torque density.

This paper is structured in four main parts. In section II, the basic structure and the design considerations of the conventional 2-rotor AFPM machine is presented. In section III, the proposed HEPM machine is presented and compared to the conventional one. In section IV, under the constraints of the voltage and the current imposed by the inverter, the characteristics of the machine in healthy and faulty modes are studied.

II. CONVENTIONAL AXIAL PM (2-ROTOR STRUCTURE)

Among the various existing structures of AFPM machine, the studied prototype is a slotted TORUS AFPM machine. It possesses one torus-shape stator sandwiched between two external rotors as shown in Fig. 1. The slotted stator structure is chosen for the reason of the time constants which impose the carrier frequency of the pulse width modulation VSI, even if the slotless TORUS AFPM machines have not cogging torque and are easier to manufacture.

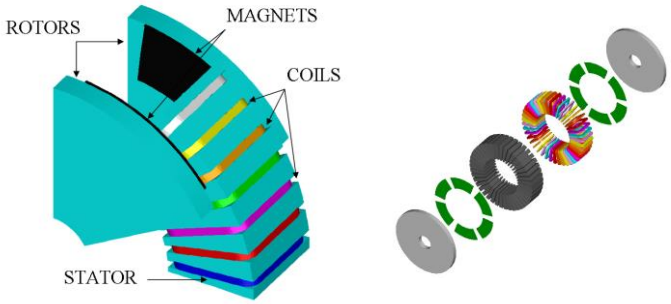

(a) one-sixth of the structure (b) exploded view

Fig. 1 Conventional TORUS AFPM

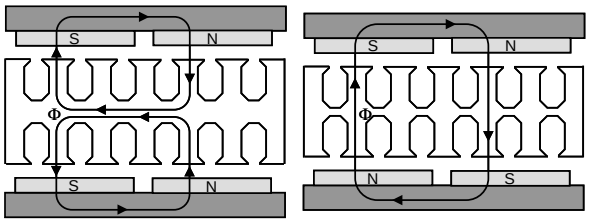

(a) NN type (b) NS type

Fig. 2 Two different topologies for TORUS-S AFPM machine [7]

Fig. 2 shows two different topologies depending on the flux paths. They are called NN type and NS type TORUS respectively. The NN type TORUS AFPM machine integrated a Gramm-Ring winding is used here, which allows adding a 3rd rotor with PMs radially magnetized and presents fewer constraints for end-winding at inner radius than the NS type TORUS-S AFPM machine. Moreover, the wingding factors for both the fundamental and the 3rd harmonic are of high values, which are related to the generation of output torque.

Fig. 3 presents the stator and the rotor of the prototype, and the main dimensions can be found in Table I. The pole-arc ratio is designed as 0.8 in order to eliminate the 5th harmonic of back-EMF, which can guarantee the high quality of torque in faulty mode operation without complex reconfiguration control [8].

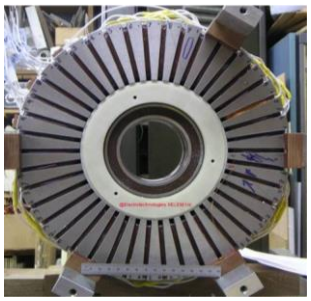

(a) stator iron

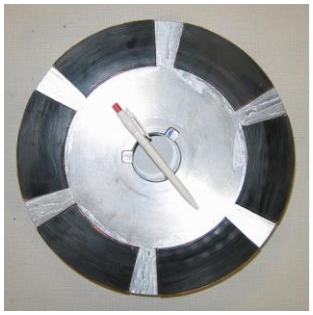

(b) rotor with PMs

Fig. 3 NN type TORUS-S AFPM machine

TABLE I
PARAMETERS AND MACHINE DIMENSIONS

Number of poles (2p)	6
Number of phases	7
Number of slots	42
Pole-arc-ratio	0.8
Core outer diameter Do (mm)	310
Axial length of stator core (mm)	78.3
Axial length of one rotor core (mm)	18.4
Axial length of one magnet (mm)	2.8
Length of one air-gap (mm)	1

The characteristics of the machine are predetermined using 3D-FEM simulation and then validated using the experimental measurements. Figure 4 shows the comparison of back-EMF. There is a relative error of 6% for the first harmonic (experimental first harmonic: 44V for 250rpm). All the harmonics are of the same order as shown in Fig. 4(b). The cancellation of the 5th harmonic is confirmed.

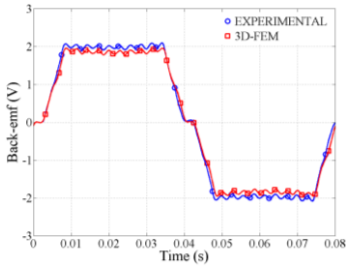

(a) back-EMF

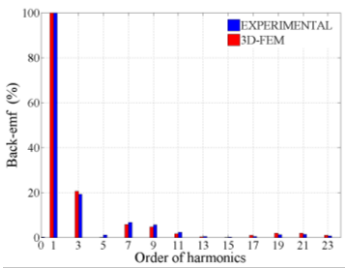

(b) harmonic spectrum of EMF

Fig. 4 Comparison of back-EMF of 2 rotor structure

III. PROPOSED HEPM (3-ROTOR STRUCTURE)

The proposed HEPM machine with TORUS-NN structure is shown in Fig. 5. Based on the conventional structure of the 2-rotor AFPM in Fig. 1, by adding a third radial rotor, the upper

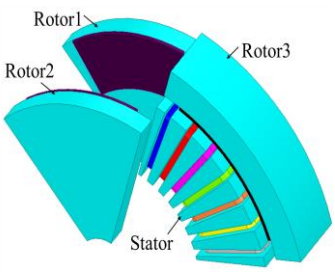

(a) FEM model

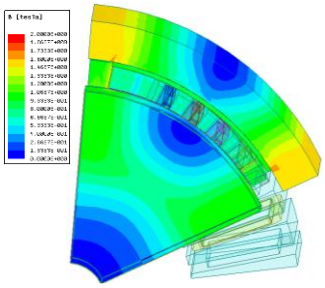

(b) flux density distribution

Fig. 5 One-sixth of the structure of the proposed AFPM

end-windings are becoming active with a significant contribution to the torque. This choice aims to transform in advantage one drawback of the NN-TORUS AFPM in comparison with the NS-TORUS AFPM, i.e. the higher value of stator back-iron.

A. Air-gap Flux Density and Back EMF

The 3D-FEM is used in the analysis to compare the performance between the conventional AFPM and the proposed HEPM. The magnetic flux density distribution with no-load is given in Fig. 5(b). In the stator core the maximum of flux magnetic density is about 1.2T and 1.6T in rotor core. Fig. 6 presents the comparison of the air gap flux density. In the air gap, the mean value of density is 0.7T with peak values at 1.1T with the conventional 2-rotor structure as shown by the blue curve. After adding the 3rd rotor in the radial direction, the mean values of densities are reduced to 0.6T for both the axial and the radial air gaps, due to the saturation of the stator iron which is made of soft magnetic material.

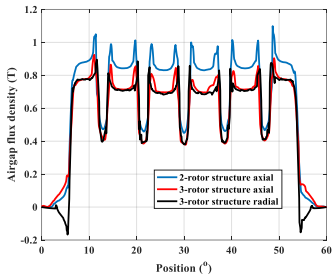

(a) Air gap flux density wave

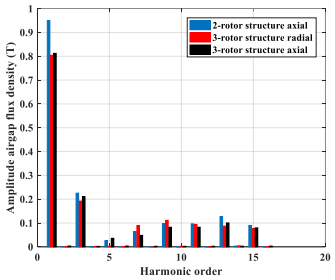

(b) harmonic spectrum

Fig. 6. Air gap flux density comparison

Fig. 7 shows the comparison of back-EMF at no-load. The amplitudes of the back-EMF for the HEPM machine are significantly increased. It can be noticed that an increase of 37.5% for the fundamental harmonic is achieved.

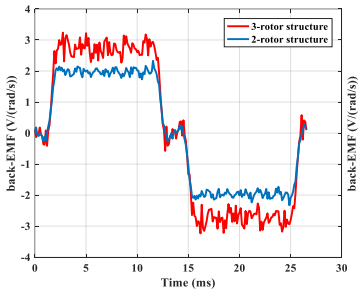

(a) back-EMF

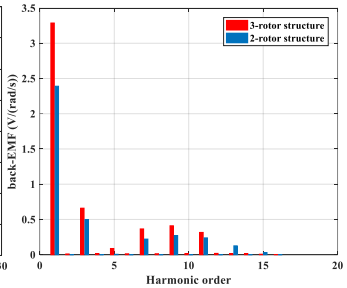

(b) harmonic spectrum of EMF

Fig. 7. Back-EMF comparison of 2 rotor and 3 rotor structure

B. Torque Density

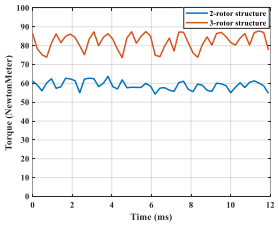

(a) Steady torque

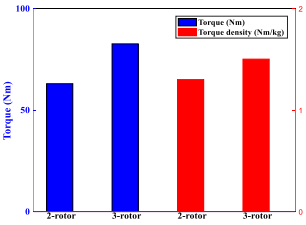

(b) torque and torque density of mass

Fig. 8. Comparison of torque and torque density of mass

Fig. 8 (a) shows the comparison of the steady torque and Fig. 8 (b) shows the comparison of the torque and the torque density of mass. Using the MTPA control strategy with the injection of the 1st and 3rd harmonic current, the output torque

and the torque density of mass for the 3-rotor structure are improved 30% and 15% respectively, compared to the 2-rotor structure.

C. Cogging Torque

The cogging torque is firstly predetermined using 3D-FEM, and then the method to reduce it is proposed and validated in this part. The blue curve in Fig. 9(a) is related to the cogging torque predetermined using 3D-FEM, and the peak value of the cogging torque (16 Nm) represents 25% of the nominal torque. A shifting of one slot (mechanical angle 4.3°) has been introduced and the cogging torque drops to 4Nm which represents 6% of the nominal one as shown in Fig. 9(a).

The cogging torque of the prototype is measured and shown in Fig. 9(b). The experimental results consist well with the 3D predeterminations and the effectiveness of the proposed method is therefore validated.

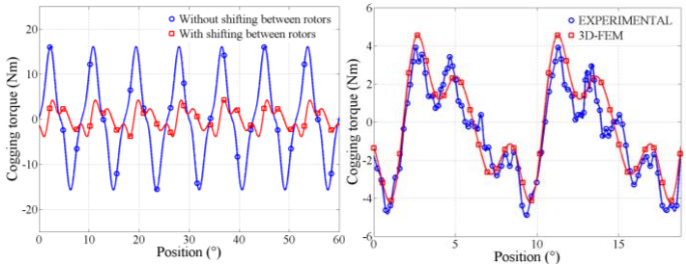

(a) FEM results with/without shifting (b) experimental validation

Fig. 9. Cogging torque characteristics with conventional 2-rotor AFPM

One degree of freedom for reducing the cogging torque is obtained thanks to the addition of the 3rd radial rotor. Fig. 10(a) shows the cogging torque with only the radial rotor, and the peak value of the cogging torque (10Nm) represents 23% of the nominal torque. Without shifting of the two axial rotors, and only the 3rd rotor is shifted one slot (mechanical angle 4.3°), the same effectiveness for reducing cogging torque can be obtained. Figure 10(b) shows the cogging torque of the complete machine, i.e. HEPM. The cogging torque (5.5Nm) represents 6.7% of the nominal torque and can be acceptable.

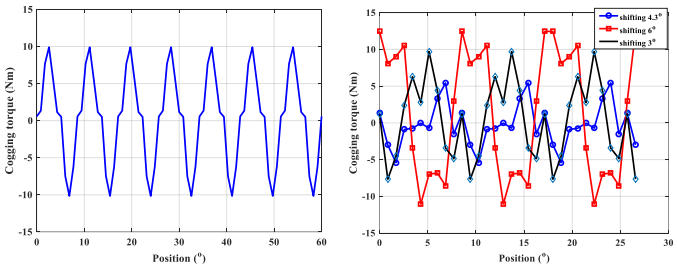

(a) with only the radial rotor (b) with 3-rotor HEPM

Fig. 10. Cogging torque characteristics with 3 rotor structure

D. Losses comparison

TABLE II
LOSSES and efficiency

	Core loss (W)	Stranded Loss (W)	Mechanical Loss (W)	Torque (Nm)	n(rpm)	P_{em} (W)	efficiency
2-rotor structure	187.25	203.85	20.00	58.79	750	4617.06	91.82%
3-rotor structure	325.91	203.84	20.00	82.74	750	6498.09	92.20%

The losses are calculated with the same rms value of current, therefore the joule losses (stranded losses here) of these two structures are of the same value. The core losses of the 3-rotor structure are higher, because the stator core are more saturated. It can be noted that, the 3-rotor structure can produce much more torque and the efficiency is higher, which proved the interest of the proposed structure.

IV. FAULT-TOLERANT CAPABILITY

In this section, the control of two structures will be presented to highlight the performance of each structure. The used algorithm is the one presented in [9] where the objective is to obtain maximum constant torques in healthy mode and single open phase fault. The constraints on current and voltage as shown in equations (1-2) are taken into account.

$$\left[|i_a|;|i_b|;|i_c|;|i_d|;|i_e|;|i_f|;|i_g|\right] \le I_{\max} \quad (1)$$

$$\left[|v_a|;|v_b|;|v_c|;|v_d|;|v_e|;|v_f|;|v_g|\right] \le V_{\max} \quad (2)$$

where ($|i_a|,|i_b|,|i_c|,|i_d|,|i_e|,|i_f|,|i_g|$) and ($|v_a|,|v_b|,|v_c|,|v_d|,|v_e|,|v_f|,|v_g|$) are absolute values of instantaneous phase currents and voltages respectively; $I_{\max}$ and $V_{\max}$ are current and voltage limits according to the converter and machine parameters.

Conventionally, voltage $V_{\max}$ is equal to a half of the DC bus voltage in the Pulse Width Modulation (PWM) technique. Current $I_{\max}$ is based on the instantaneous peak currents during a short-time operation and it is related to Voltage Source Inverter (VSI) components. In addition, the determination of $I_{\max}$ also depends on the maximum thermal currents. Based on the characteristics of the 2-axial rotor 7-phase machine given in [8], it can be assumed that $V_{\max}$=100V and $I_{\max}$=7.5A are considered.

For the sake of simplicity, especially in power constant region, only the fundamental and third harmonic components of back-EMF are considered since the amplitude of the third one is equal to about 20% of the fundamental component. The amplitudes of other higher harmonics can be neglected.

A. Healthy Mode Operation

When the machine operates in healthy condition, the optimization strategy is to calculate current references in d-q frame (i_{d1}, i_{q1}, i_{d3}, i_{q3}) by using *Fmincon* function, a nonlinear programming solver to find the minimum of constrained nonlinear multivariable functions in MATLAB. This function aims at obtaining a maximal torque and satisfying the constraints in equations (1-2).

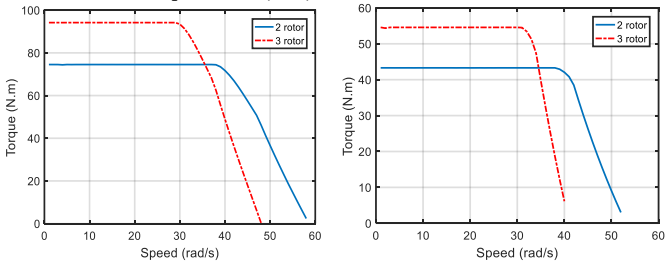

(a) healthy mode (b) single open phase fault

Fig. 11. Generated torques of the machines with 2 and 3 rotors

In figure 11(a), at low speeds, the torque generated by the 2-rotor machine is 74.53 Nm, lower than that of the 3-rotor machine with 94.18 Nm.

The imposed current and voltage are shown in figure 12(a) and figure 13(a) respectively. In constant power region, because of the higher first harmonic component of back-EMF, the 3-rotor machine has a smaller speed range and a lower torque compared to the 2-rotor one. This result confirms that the 3-rotor machine is suitable for low speed applications such as renewable energies. For high speed traction applications, the 3-rotor structure is not interesting.

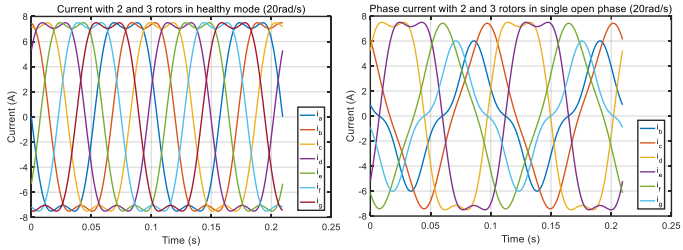

(a) healthy mode (b) single open phase fault

Fig. 12. Imposed current of the machines with 2 and 3 rotors

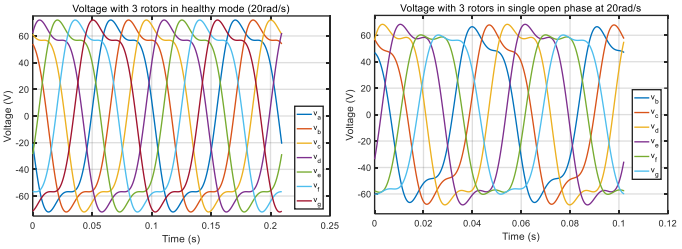

(a) healthy mode (b) single open phase fault

Fig. 13. Voltage per phase with 3-rotor

B. Faulty Mode Operation

When one phase is open-circuited, it is necessary to preserve the system operation with acceptable performances. Without loss of generality, it can be assumed that the open-circuited fault happens in phase *a*. Thus, the current in phase *a* is equal to zero. The control strategy can be adapted for other open circuit faults. The relation between currents in d-q frame and natural frame can be expressed as in equations (3-6).

$$i_{d1}^{'}=\sqrt{\frac{2}{7}}\begin{Bmatrix} i_b^{'}\cos\left(\theta-\delta\right)+i_c^{'}\cos\left(\theta-2\delta\right) \\ +i_d^{'}\cos\left(\theta-3\delta\right)+i_e^{'}\cos\left(\theta-4\delta\right) \\ +i_f^{'}\cos\left(\theta-5\delta\right)+i_g^{'}\cos\left(\theta-6\delta\right) \end{Bmatrix} \tag{3}$$

$$i_{q1}^{'}=\sqrt{\frac{2}{7}}\begin{Bmatrix} -i_b^{'}\cos\left(\theta-\delta\right)-i_c^{'}\cos\left(\theta-2\delta\right) \\ -i_d^{'}\cos\left(\theta-3\delta\right)-i_e^{'}\cos\left(\theta-4\delta\right) \\ -i_f^{'}\cos\left(\theta-5\delta\right)-i_g^{'}\cos\left(\theta-6\delta\right) \end{Bmatrix} \tag{4}$$

$$i_{d3}^{'}=\sqrt{\frac{2}{7}}\begin{Bmatrix} i_b^{'}\cos\left(3\left(\theta-\delta\right)\right)+i_c^{'}\cos\left(3\left(\theta-2\delta\right)\right) \\ +i_d^{'}\cos\left(3\left(\theta-3\delta\right)\right)+i_e^{'}\cos\left(3\left(\theta-4\delta\right)\right) \\ +i_f^{'}\cos\left(3\left(\theta-5\delta\right)\right)+i_g^{'}\cos\left(3\left(\theta-6\delta\right)\right) \end{Bmatrix} \tag{5}$$

$$i_{q3}^{'}=\sqrt{\frac{2}{7}}\begin{Bmatrix} -i_b^{'}\cos\left(3\left(\theta-\delta\right)\right)-i_c^{'}\cos\left(3\left(\theta-2\delta\right)\right) \\ -i_d^{'}\cos\left(3\left(\theta-3\delta\right)\right)-i_e^{'}\cos\left(3\left(\theta-4\delta\right)\right) \\ -i_f^{'}\cos\left(3\left(\theta-5\delta\right)\right)-i_g^{'}\cos\left(3\left(\theta-6\delta\right)\right) \end{Bmatrix} \tag{6}$$

$$i_b^{'}+i_c^{'}+i_d^{'}+i_e^{'}+i_f^{'}+i_g^{'}=0 \tag{7}$$

$$i_b^{'}+i_d^{'}+i_f^{'}=0 \tag{8}$$

Where (i_b', i_c', i_d', i_e', i_f', i_g') and (i_{d1}', i_{q1}', i_{d3}', i_{q3}') are new current references in natural and d-q frames respectively when phase a is opened; δ=2π/7 is the spatial shifting angle between adjacent phases; θ is the electrical angle.

Due to wye-connected stator windings, new current references are required to respect equation (7). There are only five equations (3-7) while six unknown currents (i_b', i_c', i_d', i_e', i_f', i_g') need to be defined. This leads to a lack of one equation to calculate the new current references. The study proposes a new simple equation as presented in equation (8) to find current solutions easily. Equation (8) ensures that the sum of each three non-adjacent phase currents is equal to zero. By imposing the current and voltage shown in figure 12(b) and figure 13(b), the torque comparison between the two machines is given where torques of 43.3 Nm and 54.6 Nm are generated by the 2-rotor and 3-rotor machines respectively before the base speed as shown in figure 11(b). With the 3-rotor machine, a torque gain of 26% has been achieved. It should be noticed that the torques of the two machines in single open phase are kept constant but decrease significantly compared to the healthy mode. After the base speed, the same behavior of torque-speed curves as in the healthy mode are obtained. The 2-rotor presents an advantage in this operating region.

V. Conclusion

In this paper, a novel 7-phase hybrid excitation permanent magnet (PM) machine has been studied. By adding the 3rd radial rotor, the torque and the torque density of mass are both improved 30% and 15% respectively. The fault tolerant capability of this machine was also validated under both the voltage and current constraints. A torque gain of 26% with 3-rotor structure has been achieved under faulty mode. The proposed HEPM was proved to be interesting in low-speed applications.

Acknowledgment

This paper was supported by the Key Development Project of Shandong Province (2017GGX30119).

References

[1] F. Barrero, M. J. Duran, "Recent advances in the design, modeling and control of multiphase machines—part 1," *IEEE Trans. Ind. Electron.*, vol. 63, no. 3, pp. 449–458, Jan. 2016.

[2] K. Wang, Z. Q. Zhu, G. Ombach, "Torque improvement of five-phase surface-mounted permanent magnet machine using third-order harmonic", *IEEE Trans. Energy Convers.*, vol. 29, no. 3, pp.735–747, Sept. 2014.

[3] A. Abdelkhalik, M. Masoud and W. Barry, "Eleven-phase induction machine: steady-state analysis and performance evaluation with harmonic injection," *IET Electr. Power Appl.*, vol. 4, no. 8, pp. 670–685, Sept. 2010.

[4] R. Zhang, J. Li, R. Qu, D. Li, “Analysis and design of triple-rotor axial-flux spoke-array vernier permanent magnet machines,” *IEEE Trans. Ind. Appl*., Vol. 54, No. 1, Oct. 2017, pp. 244-253.
[5] W. Geng, Z. Zhang, “Analysis and implementation of new ironless stator axial-flux permanent magnet machine with concentrated nonoverlapping windings,” *IEEE Trans. Energy Convers.*, Vol. 33, No. 3, Jan. 2018, pp. 1274-1284.
[6] A. Mahmoudi, N. A. Rahim, W. P. Hew, “Axial-flux permanent-magnet machine modeling, design, simulation and analysis,” *Scientific Research and Essays*, Vol. 6 (12), pp. 2525-2549, 18 June 2011
[7] F. Locment, E. Semail and F. Piriou, “Design and study of a multiphase axial-flux machine,” *IEEE Trans. Magn* , Vol. 42, No. 4, April 2006
[8] F. Locment, E. Semail, X. Kestelyn, “Vectorial approach-based control of a seven-phase axial flux machine designed for fault operation,” *IEEE Trans. Indus. Electr.*, Vol. 55, No. 10, October 2008, pp. 3682-3691.
[9] D. T. Vu, N. K. Nguyen, E. Semail, and T. J. d. S. Moraes, “Torque optimization of seven-phase BLDC machines in normal and degraded modes with constraints on current and voltage,” in *The 9th International Conference on Power Electronics, Machines and Drives*, Liverpool, UK, 2018.